Article

Optimization of Water Hyacinth Stem-Based Oxygen-Functionalized Activated Carbon for Enhanced Supercapacitors

Tilahun Temesgen, Yilkal Dessie,* Eneyew Tilahun, Lemma Teshome Tufa, Bedasa Abdisa Gonfa, Taymour A. Hamdalla, C.R. Ravikumar, and H C Ananda Murthy

Read Online

ACCESS | Metrics & More | Article Recommendations

ABSTRACT: In the current world, storing and converting energy without affecting the natural ecosystem are considered a sustainable and efficient green energy source production technology. Especially, using low-cost, environmentally friendly, and high-cycle stability activated carbon (AC) from the water hyacinth (*Eichhornia crassipes*) waste material for charge storage application is the current attractive strategy for renewable energy generation. In this study, preparation of AC from water hyacinth using a mixed chemical activation agent followed by activation time was optimized by the I-optimal coordinate exchange design model based on a 3-factor/3-level strategy under nine experimental runs. The optimum conditions to prepare AC were found to be potassium hydroxide ($\approx$17 g) and potassium carbonate ($\approx$11 g), and the carbonization time was approximately 1 h. Under these augmented conditions, the maximum specific capacitance suggested by the designed model was found to be $\approx$75.2 F/g. The regression coefficient (R^2 = 0.9979), adjusted (R^2 = 0.9917), predicted (R^2 = 0.8706), adequate precision (39.2795), and *p*-values (0.0062) proved the good correlation between actual and predicted values. The physicochemical and electrochemical properties of the final optimized AC were characterized by thermogravimetric/differential thermal analysis (TGA/DTA), X-ray diffractometry (XRD), Fourier transform infrared (FTIR), Brunauer−Emmett−Teller (BET), scanning electron microscopy−energy dispersive X-ray spectroscopy (SEM-EDS), transmission electron microscopy (TEM), high-resolution TEM (HRTEM), selected area electron diffraction (SAED), and potentiostat (CV and EIS) instruments. Finally, the optimized AC electrode after 100 cycles at a current density of 2 A g^{-1} retains an efficiency of 71.57%, indicating the good stability and sustainability of this material.
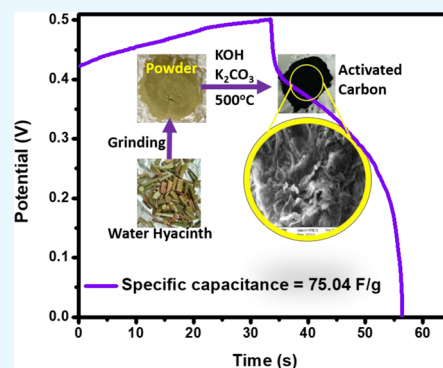
1. INTRODUCTION

Storing and transforming energy into environmentally renewable and usable forms has been considered a green and sustainable energy technology.[1,2] Due to their ability to replace nonrenewable energy sources like fossil and hydrocarbon-based fuel resources, energy generation through various storage devices like supercapacitors and batteries, as well as energy conversion devices like fuel cells, has been the focus of technology in modern human society.[3−5] Due to their extended lifespan and high power densities, special-efficiency supercapacitors are quite popular in portable digital devices; nevertheless, their low energy densities limit the range of applications that they may be used in.[6] As an alternative electrode device to address the aforementioned drawbacks, high-surface area porous carbon materials derived from biomass in the form of activated carbon (AC) are a good option because of their abundance, affordability, and environmental friendliness in addition to having the best surface area with good cycle capability and over mesoporous diameters.[7,8] However, the material of the electrode is the primary determinant of supercapacitors' efficiency. They also typically

experience a rapid decrease in specific capacitance, particularly at higher current densities.[9] Due to this reason, a variety of research has been done to generate such functioning electrode materials from many naturally available biomass carbon materials, such as lignin,[10] N-doped carbon,[11] nanosheets,[12] carbon from waste plastics, polyethylene terephthalate plastic bottle waste,[13] mixed plastics into porous carbon sheets on magnesium oxide,[14] Laminaria japonica,[15] waste straw,[16] water hyacinth,[17] *Borassus flabellifer* flower,[18] and sorghum waste,[19] which constitute some of the recent porous AC material sources.

Porous carbon-based electrode materials from water hyacinth (*Eichhornia crassipes*) stems have been widely used in supercapacitors due to their exceptional electrical con-

Table 1. Model Design Summary

factor	name	units	minimum	maximum	coded	values	mean	std. dev.
A	potassium hydroxide	g	10	20	−1.000 = 10	1.000 = 20	15	4.33013
B	potassium carbonate	g	10	20	−1.000 = 10	1.000 = 20	15	4.33013
C	carbonization time	h	1	2	−1.000 = 1	1.000 = 2	1.5	0.433013

Scheme 1. Flow Chart Diagram for the Preparation of AC from the Water Hyacinth Stem (Pictures Are Original and Organized by All the Authors)
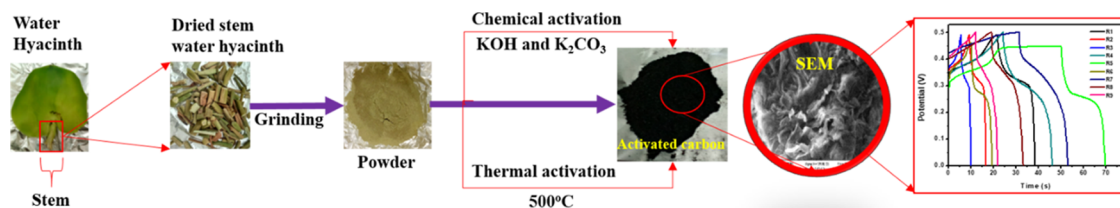
ductivity, high specific surface area, variable pore structure, and amazing physicochemical stability.[20−22] However, the charge storage performance (specific capacitance) of AC from water hyacinth is highly affected by experimental parameters (preparation factors), such as chemical activation agents and activation time.[23,24] Previously, many reports have been prepared on AC from water hyacinth using different chemical activation agents, such as K_2CO_3,[25] KOH, $ZnCl_2$, $FeCl_3$, Mg,[26] and H_3PO_4,[27] at various activation times and many others. Among these reports, none of them used a mixed chemical activation strategy and did not use any low-cost, feasible method parameter optimization strategy to produce an efficient, best-performing supercapacitor cycle performance AC device.

Moreover, to the best of our knowledge, no scientific study has been done on the process of producing AC from water hyacinth and then optimizing process factors for supercapacitors by using the response surface methodology (RSM) approach. Based on the interests of the provided variables, the RSM is a potent statistical and mathematical tool to examine interactions among elements at various levels. The RSM has therefore lately emerged as a substitute that reduces waiting times and more accurately forecasts the desired outcomes.[28] It permits maximal information to be extracted with minimal testing in a short period of time, making it an excellent choice for optimizing the manufacturing of AC from water hyacinth. In the presence of potassium hydroxide, potassium carbonate, and carbonization time, we offer the mixed chemical activation agents in this work with diverse activation times by adjusting their chemical activation mass (composition) and different activation time. Utilizing Statistical Design-Expert, Version 10.0.7.0, a three-level I-optimal coordinate exchange experimental design was employed to identify the ideal process factors and their effects on the prepared AC's characteristics, followed by the specific capacitances.

In order to maximize their interaction effects on the specific capacitance performance of AC, three levels with a three-factor parameter design and I-optimal coordinate exchange response surface methodologies were explained in this work.

2. MATERIALS AND METHODS

2.1. Experimental Design for AC Synthesis. To remove any surface contaminants, the dried water hyacinth stem that was taken from the Koka Dam, East Shewa Zone, Ethiopia, was first surface-cleansed with tap water and then rinsed with distilled water. Subsequently, the cleaned water hyacinth stem was chopped into tiny pieces (about 2 cm) and allowed to dry for a week under shade before being baked for 2 h at 90 °C.[24] By following the activation procedure with little modifications,[29] the dried stem was crushed and pulverized to get precursor samples with a particle size of 150 μm (mesh #100). Then, 15 g of precursor was treated using (10, 15, and 20 g) potassium hydroxide pellets (KOH, >85.0%, Mumbai, India) with (10, 15, and 20 g) potassium carbonate (K_2CO_3, >99.0%, Mumbai, India) in 50 mL of double-distilled water to dissolve all KOH and K_2CO_3. The mixture was left overnight at room temperature and then dried at 110 °C for 24 h.[30] To get stable pyrolysis temperature, 5.4 mg of dried sample was characterized by a DTG-60H simultaneous thermogravimetric and differential thermal analyzer from Shimadzu.

The dried material was covered by aluminum foil and set on a ceramic dish, which was then inserted in a stainless tube, and pyrolysis in the furnace was done at 1, 1.5, and 2 h at 500 °C by setting a heating rate of 5 °C min^{-1} based on the I-optimal coordinate exchange response surface design type shown in Table 1. After the pyrolysis procedure, the furnace was cooled to room temperature. After pyrolysis, the sample was milled and sieved into smaller sizes in the range of 3−5 mm. A smaller sized AC was subjected to an acid treatment by mixing 1.0 g of carbon with 100 mL to 2 M HCl solution (37%). The aqueous solution was stirred for about 1 h at 90 °C to remove as many inorganic impurities as possible. The samples were then rinsed until their pH was close to neutral and dried in a 90 °C oven for 2 h. By following the same procedure for pyrolysis and selecting 1 h optimized carbonization time and fixing the temperature at 500 °C, the conversion of the sample into carbon was done as shown in Scheme 1. Finally, AC was ready for the next measurement.

2.2. Specific Capacitance Optimization Design. The primary impacts and interactions of potassium hydroxide, potassium carbonate, and carbonization time on the particular capacitance responses were examined using an I-optimal coordinate exchange design. Table 2 shows the three factors that were constructed with three levels of process variables. A total of nine experimental runs were carried out. In order to address the acceptability of the models, the regression coefficients (R^2), adjusted (R^2), predicted (R^2), adequate precision, and p-values were studied. As one of the most affordable electrochemical capacitors, the prepared AC's

Table 2. I-Optimal Coordinate Exchange Design of Experiments for Specific Capacitance Optimization

	factor 1	factor 2	factor 3	response 1: specific capacitance (F/g)	
run order	A: potassium hydroxide (g)	B: potassium carbonate (g)	C: carbonization time (h)	actual value	predicted value
1	10	10	1	70.53	70.60
2	10	15	1.5	43.91	46.02
3	10	20	2	29.01	28.41
4	15	10	1.5	61.21	58.81
5	15	15	1	51.87	52.16
6	15	20	2	27.87	26.82
7	20	10	2	103.80	104.33
8	20	15	1.5	13.26	14.46
9	20	20	1	22.39	22.24

outstanding supercapacitive qualities make it an essential component of energy storage systems.

2.3. Characterization of AC. Thermogravimetric–differential thermal analysis (TGA-DTA) was carried out using a DTG-60H detector (Shimadzu, Japan) under nitrogen gas. The crystalline structure was characterized using an X-ray diffractometer (SHIMADZU, XRD-7000) at a voltage of 40 kV and a current of 30 mA using (Cu $K\alpha$ = 1.5406 Å) radiation as an X-ray source. Its scanning rate was performed at $2°$ min^{-1} in the 2θ range from 10 to 80°. The intermolecular bonding vibration and stretching motion were characterized by Fourier transform infrared (FTIR) spectra with a PerkinElmer FT-IR BX spectrophotometer in the range of 4000–400 cm^{-1} with samples prepared using KBr pellets. Scanning electron microscopy with energy dispersive X-ray spectroscopy (SEM-EDX-EVO 18 model, low-vacuum facility, ALTO 1000 Cryo attachment) was used to understand the surface topography and chemical elements of the prepared materials. The microstructural morphology, crystalline size distribution, and purity of the synthesized NPs were elucidated using TEM, HRTEM, and SAED micrographs with a JEOL TEM 2100 HRTEM machine.

2.4. Electrode Preparation. Rectangular-shaped Ni foam (2 cm × 1 cm) as a current collector was first etched using 1 M HCl for 30 min in order to remove surface oxides and impurities.[31] The etched Ni foam was then rinsed thoroughly with distilled water and ethanol and then dried at room temperature. Modification of the electrode using AC was performed by following the previous report with convinced modifications.[32] Briefly, electrode fabrication was done by preparing a paste from the mixing of AC materials and poly(vinyl alcohol) (PVA) as a binding agent in 9:1 ratio by mass. First, 10 mg of binder was placed in a 100 mL beaker, and 10 mL of distilled water was added to it. In order to dissolve the PVA completely, the solution was placed on a hot plate and continuously stirred at 45 °C for 2 h. After that, 90 mg of the active AC sample was thoroughly ground in a mortar to get a fine powder, and then, 250 μL of the already prepared PVA solution was added in order to disperse the active material. Further, only 1 cm^2 of the etched Ni foam was covered homogeneously by applying about 100 μL of the slurry using a micropipette and drying at 70 °C overnight. Mass was measured before and after mass loading of the active material by a four-digit electronic balance for electrochemical measurements.

2.5. Electrochemical Measurements and Performance Test. All electrochemical characterizations were performed in a standard three-electrode system using an IVIUM potentiostat while using the as-synthesized AC electrode as a working electrode (WE), Pt wire as the counter electrode (CE), and Ag/AgCl electrode as the reference electrode (RE) in the presence of a 1 M KOH electrolyte solution. The cyclic voltammetry (CV) experiments were performed at varying scan rates from 10 to 100 mV s^{-1} at the range of (0–0.5 V). The galvanostatic charge/discharge (GCD) tests were recorded from 1 to 10 A g^{-1} current density in the voltage window (0–0.5 V). Electrochemical impedance spectroscopy (EIS) was performed at 10 mV voltage in the frequency range from 100 kHz to 0.01 Hz.

3. RESULTS AND DISCUSSION

3.1. Specific Capacitance Performance Test. Specific capacitance is usually valued through a GCD measurement. Hence, nine GCD runs at a current density of 2 A g^{-1} were carried out to study the electrochemical performance of the prepared AC, as shown in Figure 1. The potential charge and
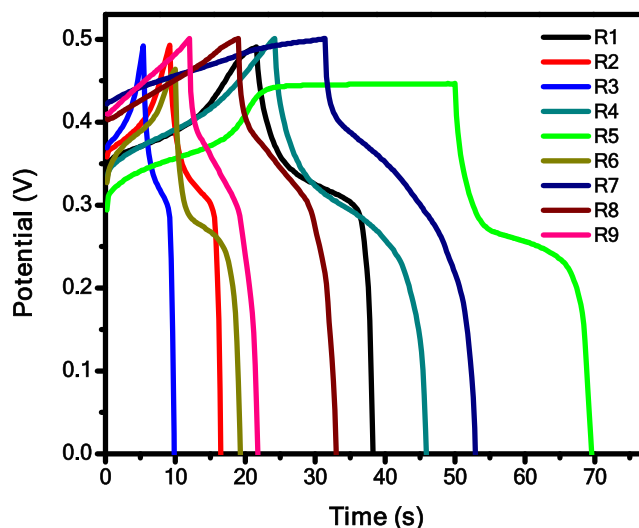

Figure 1. Comparison of the galvanostatic charge and discharge curve at the current density of 2 A g^{-1}.

discharge curves as a function of time have an almost triangular shape with minimal deviation (i.e., an asymmetrical triangle curve), which is consistent with the typical behavior of a redox-type (faradaic) electrochemical storage mechanism because ions in the electrolyte can both enter the pore structure for storage and react quickly with the material's surface at low discharge times, increasing specific capacitance at high discharge times for the majority of runs. In other words, an AC-modified electrode may be able to store charge by simultaneously causing a surface redox reaction at the electrode–electrolyte interface and the reversible adsorption/desorption of electrolyte ions. Consequently, the system developed an asymmetric storage mechanism in every run, demonstrating the presence of quick ion diffusion, low internal resistance, and superior charge and discharge reversibility.[33,34] However, run R5 (the R5 sample) could not be charged to 0.5 V, which might be due to both voltage-independent parallel leakage resistance and electrolyte decomposition as well as electrolyte crystallization on the working electrode,[35] and its

Table 3. ANOVA Analysis for the 2FI Model[a]

source	sum of squares	df	mean square	F-value	p-value	
model	6435.19	6	1072.53	159.36	0.0062	significant
A, potassium hydroxide	3.06	1	3.06	0.4541	0.5698	
B, potassium carbonate	360.57	1	360.57	53.57	0.0182	
C, carbonization time	67.36	1	67.36	10.01	0.0871	
AB	235.53	1	235.53	35.00	0.0274	
AC	957.63	1	957.63	142.29	0.0070	
BC	14.22	1	14.22	2.11	0.2832	
residual	13.46	2	6.73			
corrected total sum of squares	6448.65	8				
adequate precision	39.2795					
R^2	0.9979					
adjusted R^2	0.9917					
predicted R^2	0.8706					

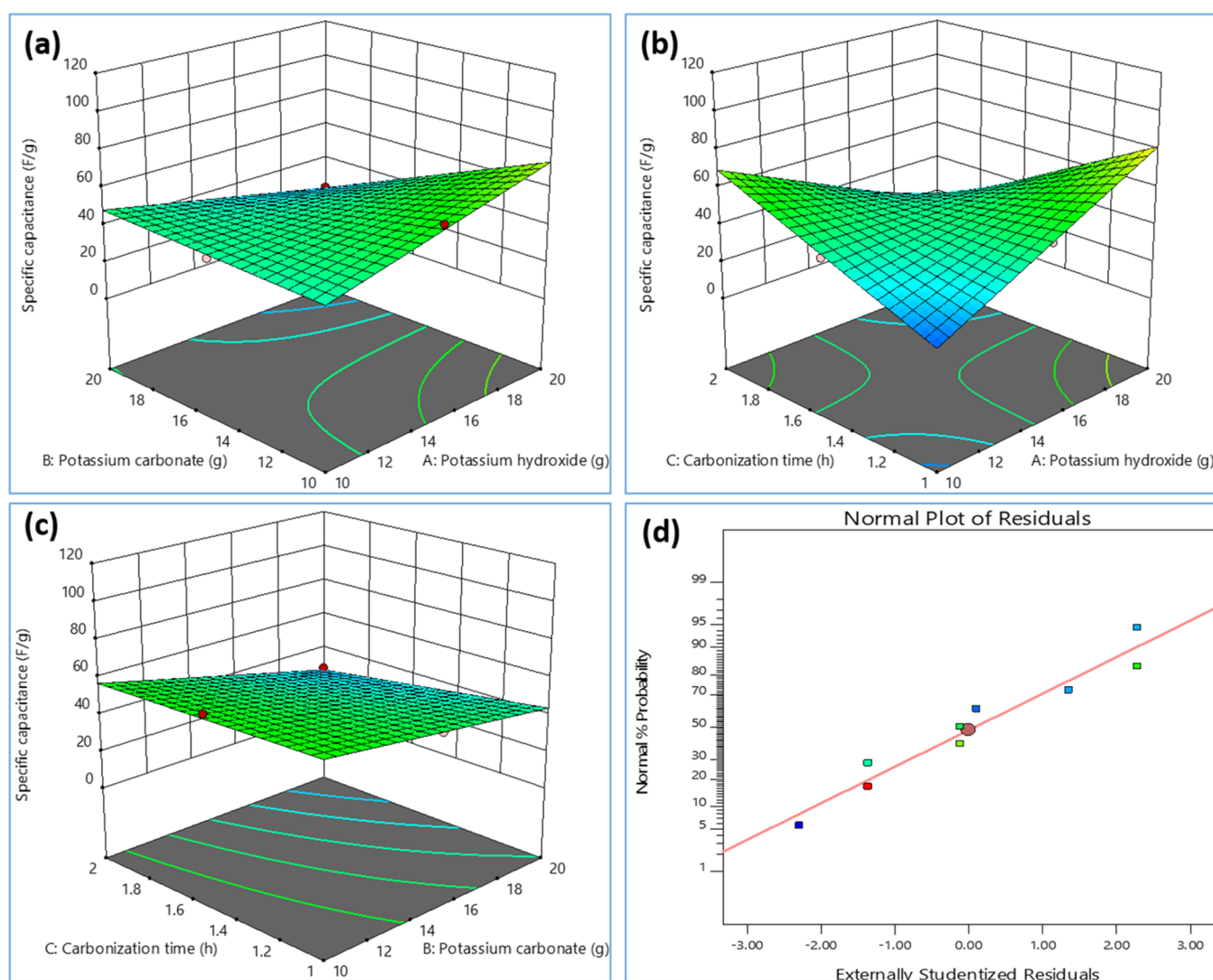[a]df = degree of freedom.

Figure 2. 3D surface plots and their interaction effects between (a) potassium hydroxide and potassium carbonate, (b) potassium hydroxide and carbonization time, (c) potassium carbonate and carbonization time, and (d) residuals of normal plot.

charging−discharging behavior is restricted to a voltage near 0.45 V. Thus, for run 5 (R5), there is a quite long charging platform. The specific capacitance (C_s) of nine runs was calculated using eq 1[36]

$$C_s = \frac{i \Delta t}{m \Delta V}$$

(1)

Where i is the discharge current, Δt is the discharge time, m is the mass of the active material in the electrode, and ΔV is the
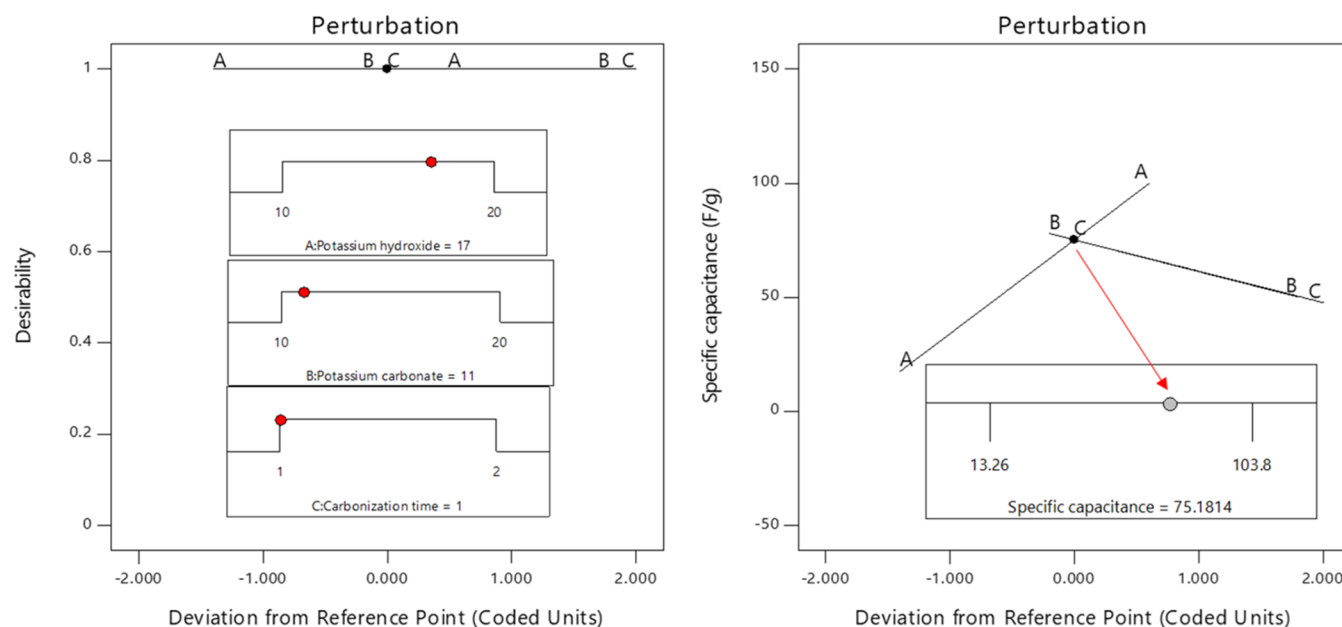
Figure 3. Perturbation at desirability = 1.

potential window of cycling. The actual and predicted specific capacitance values are shown in Table 2.

From the analysis of variance (ANOVA) analysis (Table 3), the quadratic equation elucidated by I-optimal coordinate exchange confirmed that the model F-value of 159.36 implies that the model is significant. There is only a 0.62% chance that an F-value this large could occur due to noise. P-values less than 0.0500 indicate that model terms are significant. In this case, B, AB, and AC are significant model terms. The predicted R^2 of 0.8706 is in reasonable agreement with the adjusted R^2 of 0.9917, i.e., the difference is less than 0.2. Adequate precision measures the signal-to-noise ratio. A ratio greater than 4 is believed to be significant. A ratio of 39.279 indicates an adequate signal. This model can be used to navigate the design space. Hence, it is suggested that the experimental parameter with the highest F-value from Table 3 is potassium carbonate, and this parameter is the most influential factor that affects the synthesized AC.

Control independent (parameter) variables and their corresponding sensitivity charge storage capacity responses served as the foundation for a two-factor interaction (2FI) model function that was created to forecast the particular capacitance performance test. Using an I-optimal coordinate exchange design-type model with a two-sided confidence level of 95%, the model's coefficients were well calculated. Equation 2 provides the mathematical expression of the specified model function. This formula expresses and forecasts the effects of the three independent variables on specific capacitance (SC) performances in terms of coded factors.

$$SC = +47.09 + 1.08A - 11.72B - 5.07C - 14.21AB$$
$$- 28.65AC - 3.49BC \qquad (2)$$

The equation in terms of coded factors can be used to make predictions about the response at given levels of each factor. The coefficients of AC, AB, B, C, and BC were higher compared to the coefficients of A. This suggests that variations in the interaction between potassium hydroxide and carbonization time have a significant impact on the charge storage capacity of AC. During the activation phase, potassium

hydroxide and potassium carbonate react with the carbonaceous matrix to form a significant number of functional groups, some of which include oxygen. Oxygen atoms have the ability to effectively maximize AC wettability, increasing its capacity to store additional charge. However, if the positive coefficient of A indicates that potassium hydroxide has a positive effect as its mass grows, then, the impact of individual potassium carbonate on specific capacitance has a dominant effect on the charge storage capability of AC. When moderate potassium carbonate is added to create oxygen-functionalized AC, this effectiveness lasts forever.

3.2. Optimization of Parameters for AC Preparation. Figure 2 illustrates the important influences of potassium hydroxide, potassium carbonate, and carbonization time on the specific capacitance of AC. Figure 2a shows that the specific capacity of AC increases with a fixed carbonization period when the mass of potassium hydroxide is increased and that the mass of potassium carbonate is low. On the other hand, Figure 2b illustrates a noteworthy effect on specific capacitance. As Figure 2c illustrates, the relationship between carbonization time and potassium carbonate did not materially alter AC's storage capacity. The positive and negative externally studentized residual distribution across the straight line shown in Figure 2d suggests that the designed models are adequate between actual (experimental) and predicted values. Furthermore, to elucidate the degree of charge storage capability of AC behind each parameter, the F-values of the model help to prioritize the dominance of the factor that affects the designed experimental run. Keeping this order of influences as shown in Table 3, the preparation of AC is highly influenced by B, potassium carbonate > C, carbonization time > A, potassium hydroxide. Thus, according to the order, the mass of potassium carbonate has the dominant and most significant effect, while carbonization time has the least effect on AC charge storage capacity. Potassium carbonate was added in excess in this order, which resulted in excessive activation, but it also may have contributed to pore collapse and the breakdown of the multilayer structure.[8] Thus, the produced
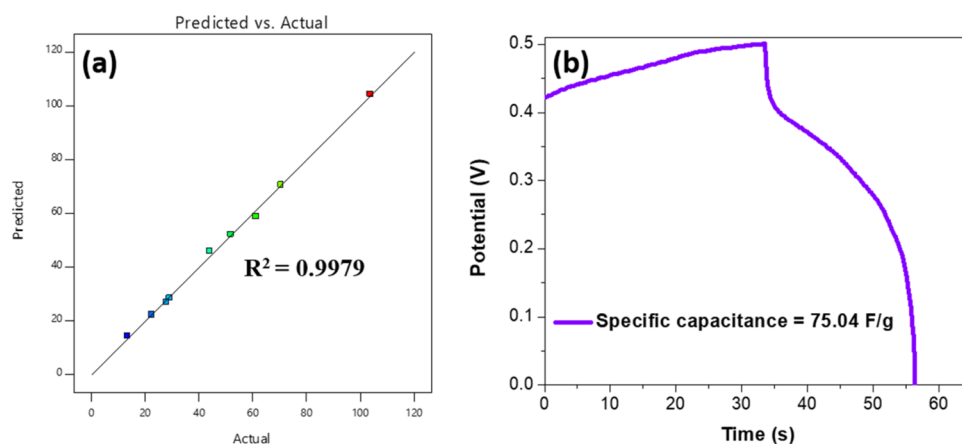
Figure 4. Relationship between actual and predicted values of optimized AC preparation for the effective charge storage capacity.
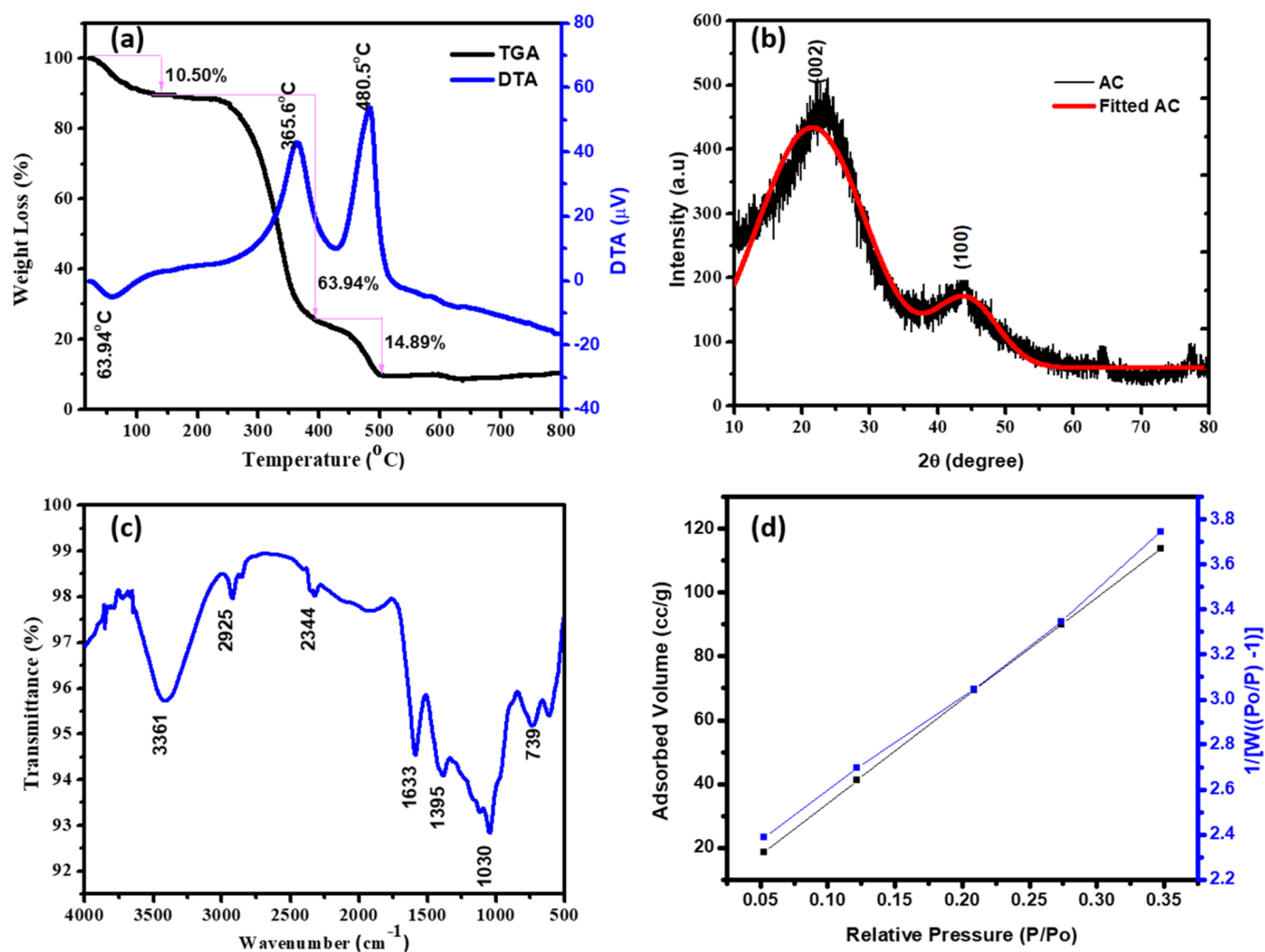

Figure 5. (a) TGA/DTA thermograms, (b) XRD patterns, (c) FTIR spectra, and (d) BET nitrogen adsorption/desorption isotherm surface area analysis for optimized AC.

AC was optimally synergistically activated with a suitable amount of potassium carbonate.

As a result, the optimum conditions to prepare AC were found to be potassium hydroxide ≈17 g, potassium carbonate ≈11 g, and carbonization time ≈1 h. Under these optimum conditions, the maximum specific capacitance suggested by the designed model was found to be ≈75.2 F/g at unity

desirability, as shown in Figure 3. Since the desirability value varies between 0 and 1, depending on the proximity of the outputs to the required specific capacitance, ≈75.2 F/g at a desirability of 1 indicated that the model is 100% predictive to give the required target and to get the optimized experimental parameters. Therefore, the optimized three parameters found

in the inset of Figure 3 produce the most accurate and precise results at maximum desirability.

3.3. Model Validation. The model validation was performed by using two sets of techniques. First, the closer relationship between the actual and predicted correlation coefficients shown in Figure 4a. Thus, the regression coefficient (R^2) was found to be 0.9979. The relation suggests that the proposed model is effectively developed with effective correlations among all parameters for AC preparation. The second way of validating a test is by preparing AC using optimized experimental parameters. Briefly, 15 g of precursors was treated using 17 g of KOH and 11 g of K_2CO_3 in 50 mL of double-distilled water to dissolve all KOH and K_2CO_3. The mixture was left overnight at room temperature and then dried at 110 °C for 24 h. To get a stable pyrolysis temperature, 5.4 mg of the dried sample TGA/DTA was obtained by a DTG-60H. Then, the dried material was covered by aluminum foil and set on a ceramic boat, which was then inserted in a stainless tube, and pyrolysis in the furnace was done for 1 h at 500 °C by setting a heating rate of 5 °C min^{-1}. After the pyrolysis, the furnace was cooled to room temperature. After pyrolysis, the sample was milled and sieved into smaller sizes in the range of 3−5 mm. A smaller sized AC was subjected to an acid treatment by mixing 1.0 g of carbon with 100 mL to 2 M HCl solution (37%). The aqueous solution was stirred for about 1 h at 90 °C to remove as many inorganic impurities as possible. The samples were then rinsed until their pH was close to neutral and dried in a 90 °C oven for 2 h. By following the same procedure for pyrolysis, selecting 1 h optimized carbonization time and fixing the temperature at 500 °C, the conversion of the sample into carbon was done. Finally, the prepared AC was tested for supercapacitors at 2 A g^{-1} and 6 M KOH, and its specific capacitance was found to be 75.04 F/g with a difference of 0.16 (16% error), which was lower than 0.2 or 20% error values. Since the 0.2 numerical value is a standard value in Design-Expert 10 (File Version 10.0.7.0) software, from this validation, it is found that the model is adequate for the optimization of three operational parameters. Using the same electrolytes with 6 M KOH, similar work was done by other biomass-based AC, such as chestnut AC,[37] purple corncob AC,[38] (husk, fiber, grain, and cob),[39] Metaplexis japonica-based AC.[40]

3.4. Analysis of Optimized AC. The TGA/DTA of three major stages was also observed in the thermal degradation components of water hyacinth-based AC samples, as depicted in Figure 5a. The first stage, which started from room temperature to 120 °C, involved the removal of surface-adsorbed moisture content present within the pores of water hyacinth, with approximately 10.5% weight loss. The most weight loss (63.94%) with two DTA endothermic peaks was observed at about 365.6 and 480.5 °C in the second stage, which depicts the combined decomposition of the hemi-celluloses and cellulose molecules, respectively.[41] The third and last stage of decomposition, which occurred above 400 °C, was due to the lignin degradation process.[42] Above 500 °C, no weight loss was observed, and as a result, it was fixed as the carbonization temperature for AC preparation. The results showed good agreement with the previously reported work.[43,44]

XRD pattern analysis of the AC material was carried out to examine its crystalline structure. From Figure 5b, the existence of broad peaks at about 2θ = 24.12 and 43.60° in the XRD pattern of AC is allocated to the amorphous structure and corresponds to the (002) and (100) planes of AC, respectively. However, some additional minor peaks were still observed, which might be due possibly to that some chemical activating agents were not completely removed during washing procedures to neutralize the produced AC.[45]

The FTIR analysis is depicted in Figure 5c, and the prepared AC sample showed a broad absorption band in its FTIR spectrum peak at about 3361 cm^{-1}. This is mainly the characteristic peak of the stretching vibration band of the −OH bond in physically adsorbed moisture-containing surface water molecules.[46] For chemical adsorption, these oxygen functional groups serve as active sites. The peak that is present at 1633 cm^{-1} represents the bond stretching for the C−C, and the peak at 2925 cm^{-1} is ascribed to the existence of aliphatic bond stretching for the −CH$_2$ groups (Mojoudi et al.). Finally, 1030 cm^{-1} might be related to the OH bending vibration.[47] The band found at 739 cm^{-1} is related to the stretching vibrations of the C−H out-of-plane band.[47]

A surface study of the AC was carried out using Brunauer−Emmett−Teller (BET) analysis and showed good surface properties. Specific surface area (SSA) measurements of the synthesized material were performed using a BET analyzer via a nitrogen adsorption isotherm at 77 K, with the results of SSA having a value of 522.499 m^2/g as shown in Figure 5d. Its estimated cumulative pore volume and average pore radius were found to be 0.16 cm^3 g^{-1} and 0.92 nm, respectively. This could be a good indication of the use of KOH as an activating agent for porosity size improvement.[48] It has been clearly shown that the SSA is influenced by the chemical activation agent's composition. SSA and the pore volume have a direct effect on the electroactive properties of the electrode material in supercapacitor applications. The kind of carbon source biomass precursors used or the activation parameters, such as the activation agent-to-carbon ratio, and the synergistic effects of the high-temperature activation method determine the pore shape.[49] It is established from previously published work that the best materials for SC use include high-SSA, interconnected pores of various shapes and micropores with larger volumes and diameters that are closer to the size of electrolyte ions.[50]

All of the pore structures have various roles in the electrochemical charge/discharge process. For example, the macropore structure serves as the ion buffer reservoir for the micro- and mesopore structures. High performance in supercapacitors is made possible by the abundance of ion transport channels provided by mesopores and the availability of ion storage sites provided by micropores.[51] According to the literature, micropores with larger diameters and volumes that are closer to ion sizes as well as interconnected pores with varying configurations are favored for use as supercapacitor electrodes. According to eq 1 above, as pore size is raised, the average distance between the pore wall and the center of the ion increases and the capacitance falls. On the other hand, capacitance rises when the pore size is reduced because of a decrease in the average distance between the pore wall and the ion center.[52] Generally, the synergistic activation mechanisms of potassium carbonate and hydroxide in the activation of microporous carbon can be summed up in three ways:[53] (i) the chemical etching is caused by the activating chemicals' redox reaction, which consumes the basal carbon and forms pore structures; (ii) the heating process produces H_2O (g) and CO_2 (g), which enhances the activated carbon's porosity properties; and (iii) K ions are readily available from KOH and K_2CO_3. During the process, the previously described chemical
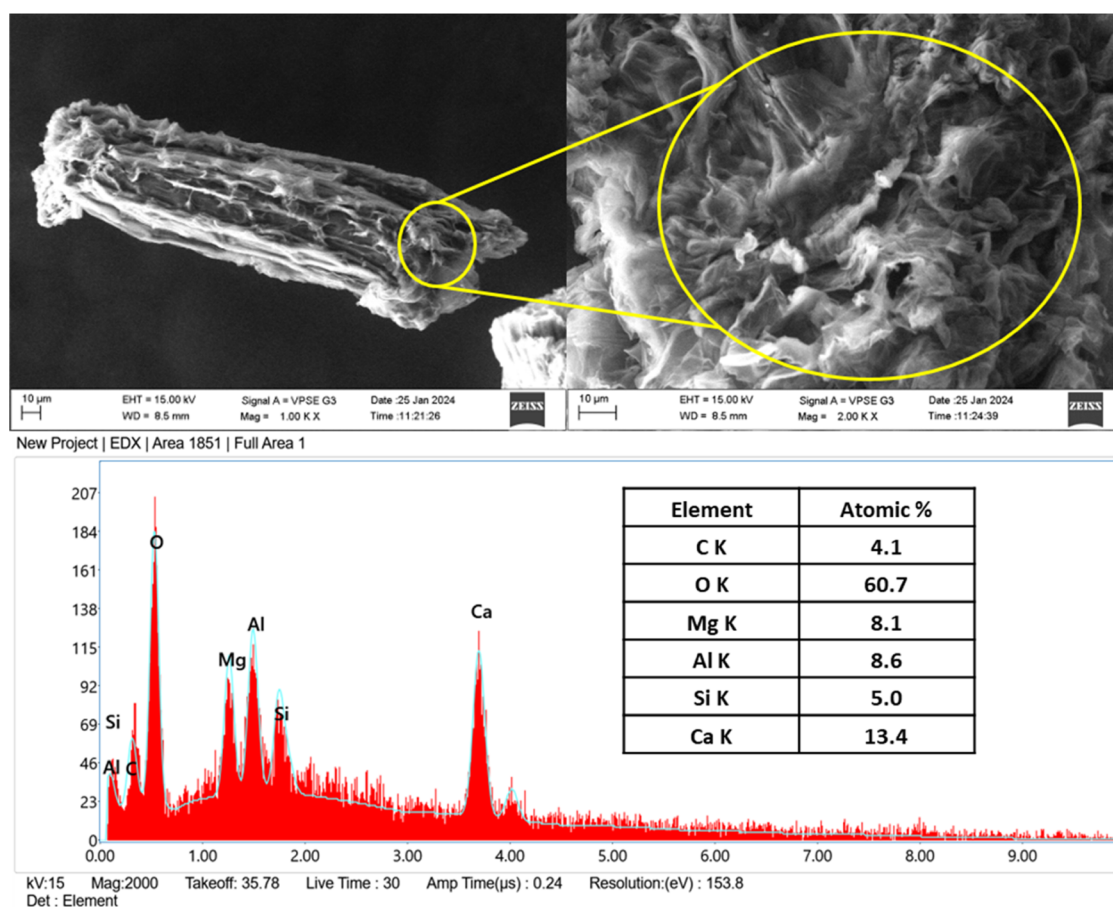
Figure 6. SEM-EDX analysis of the optimized AC.
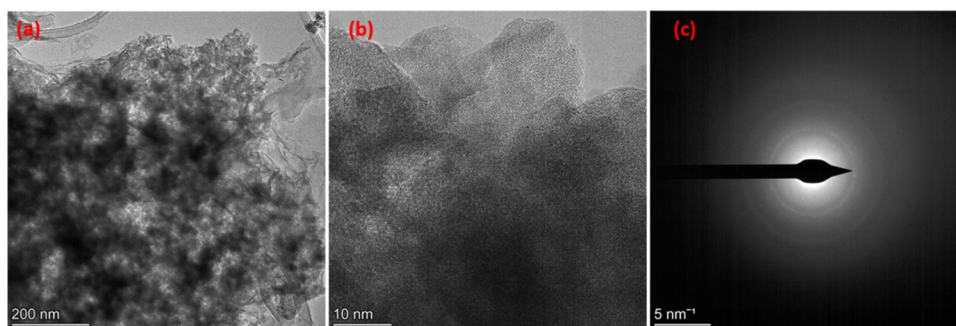

Figure 7. (a) TEM, (b) HRTEM micrographs, and (c) SAED pattern of the optimized AC.

intercalates into the carbon lattice, breaking down the lattice's structure. Ultimately, the washing process can remove these K ions and other inorganic impurities, which is why AC exhibits a noteworthy SSA.

Energy dispersive X-ray spectroscopy (EDX) in conjunction with scanning electron microscopy (SEM) was used to analyze the morphology of KOH- and K_2CO_3-treated AC particles. The shape of the AC produced at 500 °C is displayed in Figure 6. The obtained SEM image showed that the AC's outside surface was highly erratic and covered in numerous voids of varying sizes. This may occur as a result of the activation process's production of different volatile materials.[47] Primarily, the surface morphology of the fabricated C was discovered to consist of a combination of irregular pieces and microsized pores with interconnected networks resembling thin sheets in nature, together with high porous surface phenomena.[54]

Figure 6 displays the indicated EDX elemental analysis for the C and O existence in the ready AC. Based on the quantification of the peaks, the atomic percentages of C and O were determined to be around 4.1 and 60.7, respectively. Alkali and alkaline earth metals were present, along with a comparatively high 64.8% carbon and oxygen atomic content, which suggested a low carbonization process and ineffective washing steps throughout the chemical modification process.[47] However, because of their pseudocapacitance nature and consequent enhancement of the redox process of AC, the presence of additional metallic impurities in the manufactured AC may have the benefit of improving AC supercapacitor performance.[55] Furthermore, if metallic impurities are present in small enough quantities in terms of atomic percent, they may serve as great active sites that facilitate both excellent charge storage capacity and electrocatalytic activity.[33] As a
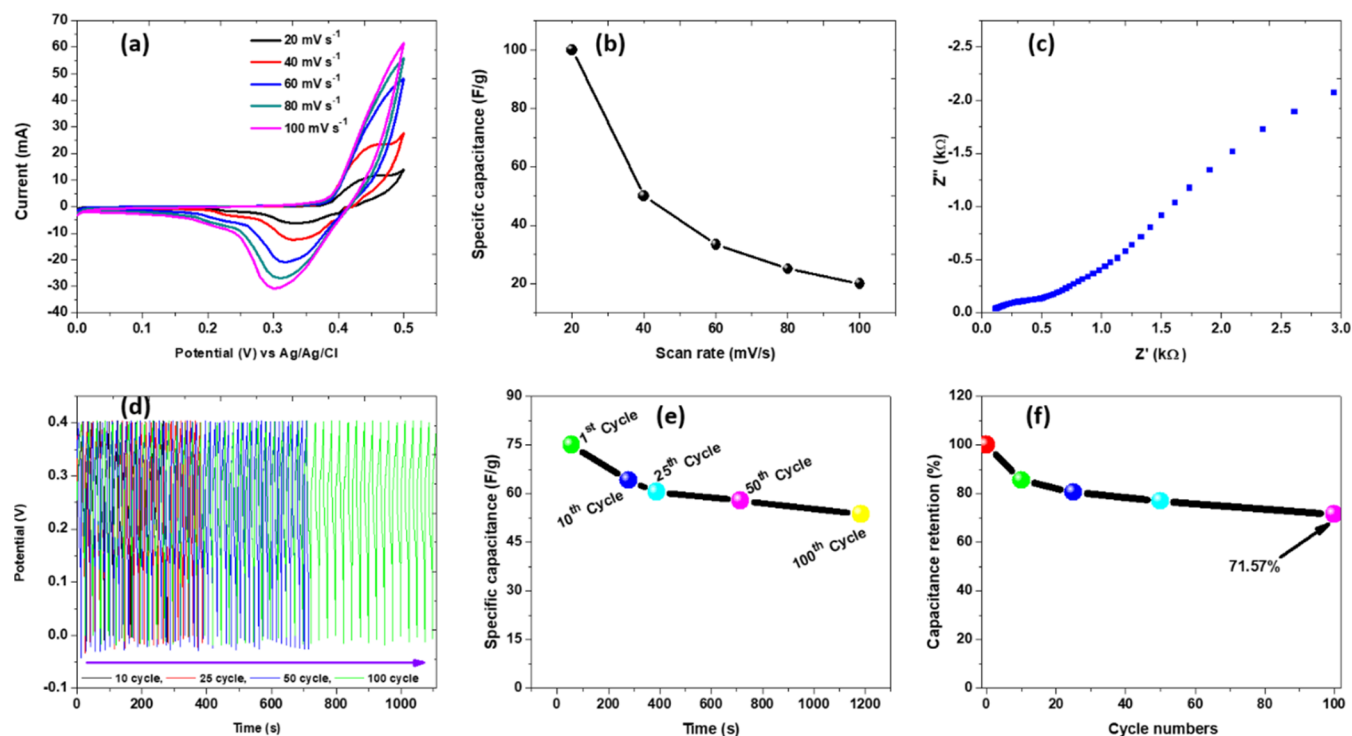
Figure 8. (a) Cyclic voltammetry of AC at different scan rates of 20, 40, 60, 80, and 100 mV s^{-1}, (b) specific capacitance versus scan rates at 2 A g^{-1}, (c) Nyquist plot after applying a sinusoidal wave with amplitude of 10 mV over the frequency range from 100 kHz to 0.01 Hz (d) cyclic stability for over 100 cycles from GCD, (e) specific capacitance versus cycle time plot from GCD, and (f) cyclic stability versus number of cycles over 100 cycles from GCD in 6 M KOH solution.

result, the prepared AC device's surface offered greater delocalized charge accumulation and supported the quick charge storage mechanism.[56]

After chemical activation with KOH and K$_2$CO$_3$, Figure 7a shows the TEM image of the nanosized AC produced from aqueous *E. crassipes* at a magnification of 200 nm. The TEM grid's particle grain size boundaries, which are apparent in Figure 7a, show that the loss of more volatile chemicals caused the majority of the particles to shrink to sizes between 30 and 185 nm. Furthermore, because of its hierarchical micro-mesoporous nature, the TEM morphology further supports the production of aggregated AC with a porous structure and a variety of voids.[57] The absence of lattice fringes in the HRTEM image seen in Figure 7b suggests that AC is amorphous.[8] The selected area electron diffraction (SAED) pattern, which is seen in Figure 7c, further supported this. Given that the SAED pattern shows no white circular spots, it may be concluded with certainty that the modified AC was primarily aggregated and agglomerated.

3.5. Electrochemical Characterization and Supercapacitor Stability Test. The current response of redox-active solutions to a linearly cyclic potential sweep is measured using the electrochemical technique known as CV, which is then shown as measured current versus applied potential. The AC electrode's CV curves at various scan rates, spanning from 20 to 100 mV s^{-1}, are displayed in Figure 8a. Even at a very high scan rate of 100 mV s^{-1}, the electrode demonstrated good retention (redox behavior), as is reported. It is well known that the Ni foam surface underwent modifications to AC. Ni foam functions as a current collector and experiences both oxidation (0.55 V) and reduction (0.46 V) peak potentials in an alkaline solution such as KOH. The redox peak arises from the faradaic reaction of Ni(OH)$_2$, as evidenced in the literature[58] and

shown in eq 3. Therefore, it is evident from the voltammogram curve that the alteration of the Ni foam by AC is what caused the shift in both the oxidation and reduction peaks to a negative potential at low scan rates. Assuming the integration of oxygen heteroatoms into the AC matrix, further physical and chemical features of AC may result. As a result, oxygen-functionalized AC, which has a carbonyl functional group formed on its surface, may aid in reversible redox reactions and enhance the supercapacitor performance without impairing cycle performance. Eq 4 illustrates how the oxygen-containing functional group in the AC in KOH electrolytes, as reported in the literature, promotes faradaic redox processes throughout the charging–discharging time.[59]

$$\mathrm{Ni(OH)_2 + OH^- \rightleftharpoons NiOOH + H_2O + e^-} \tag{3}$$

$$\mathrm{-C=O + H_2O + 2e^- \rightleftharpoons -CH-O^- + OH^-} \tag{4}$$
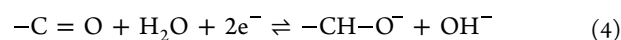
This suggests that the AC working electrode that was created is excellent in terms of both stability and performance. Therefore, the excellent reversibility and high-speed capabilities of the synthesized electrode materials were validated by the linear dependency of peak current on scan rates.[8] The potentials of the anodic and cathodic peaks, however, shift somewhat to the more positive and negative sides as the scan rate increases. This phenomenon may be related to electrode polarization because of the rapid ionic and electronic processes at the electrode's surface. Figure 8b displays the computed specific capacitance against the scan rate. The electrode produced a maximum specific capacitance of 100 F g^{-1} at 20 mV s^{-1}. As predicted, the specific capacitance dropped with an increase in the scan rate.

Using EIS, the electrodes' comprehensive electrochemical performances were examined in further depth. Figure 8c

displays the AC electrode's resulting Nyquist plots. The contributions of contact (polarization) resistance between the electrode/electrolyte interface and interfacial charge transfer resistance during diffusion or transport of the electrolyte into the porous carbon electrode are responsible for the plot's incomplete semicircle in the high-frequency region. Furthermore, as documented in the literature, the parallel combination of capacitive behavior and resistance in the high-frequency domain was also responsible for the incomplete semicircle's development.[60] The induced charge transfer resistance linked to the electrode–electrolyte ion chemical interaction is thus demonstrated by the existence of such a semicircle in this frequency range. Higher electron transfer resistance, an indicator of the material's poor conductivity, is indicated by the semicircle's bigger diameter.[8] On the other hand, ionic diffusion resistance is shown by the existence of a straight line in low-frequency regions when the ions from the electrolyte move into the pores of the electrode material. Ions can effectively diffuse into the micropores through a linear zone with a steep slope that corresponds to the electrodes. The plot's inclusion of a straight line and semicircle, respectively, indicates the investigated electrode's resistive and capacitive characteristics. Moreover, the figure indicates that the property responsible for the improved charge storage efficiency was the higher charge transmission rate between the electrolyte and the porous AC electrode.[41] As a result, 277 Ω was determined to be the charge transfer resistance value. The potential fluctuation as a function of the charging–discharge duration at 10, 25, 50, and 100 cycles at a current density of 2 A g^{-1} is displayed in Figure 8d. As seen in Figure 8e, the electrode material continues to hold for a long period of time, even after 100 cycles. Figure 8f displays a capacitance retention value of 71.57%, demonstrating the good stability and sustainability of this material.

4. CONCLUSIONS

The analysis of experimental design through RSM (I-optimal coordinate exchange design model based on a 3-factor/3-level strategy under nine experimental runs) was used to study the three parameters (factors), such as potassium hydroxide, potassium carbonate, and carbonization time, on the specific capacitances as responses toward the preparation of our AC. The influences of three factors and their interactions on specific capacitances have been modeled by the two-factor interaction (2FI) model function. The optimum conditions to prepare an optimized AC from the water hyacinth stem were found to be potassium hydroxide ≈17 g, potassium carbonate ≈11 g, and carbonization time ≈1 h. Under these conditions, model validation was performed, and the prepared AC was tested for supercapacitors at 2 A.g^{-1} and 6 M KOH, and its specific capacitance measured experimentally at optimum conditions was found to be 75.04 F/g with a difference of 0.16 (16% error) from the suggested model specific capacitance of 75.2 F/g, which was lower than 0.2 or 20% error values. This is due to the surface structure and electrochemical property modification of AC with a SSA of 522.499 m^2/g, a cumulative pore volume of 0.16 cm^3 g^{-1}, and an average pore radius of 0.92 nm. The lower charge transfer resistance value of 277 Ω associated with the modified and optimized AC enhances the charge storage proficiency with a capacitance retention of 71.57%, indicating the good stability and sustainability of this material. Therefore, from this validation, it is concluded that the model was adequate for

the optimization of three operational parameters to produce stable pores of AC-based electrode materials from low-cost water hyacinth waste stem materials.

■ AUTHOR INFORMATION

Corresponding Author

Yilkal Dessie − *Department of Applied Chemistry, School of Applied Natural Science, Adama Science and Technology University, 1888 Adama, Ethiopia;* ◉ orcid.org/0000-0001-7287-6499; Email: yilikaldessie@gmail.com

Authors

Tilahun Temesgen − *Chemistry Department, School of Natural Science, Dambi Dollo University, 260 Dambi Dollo, Ethiopia*

Eneyew Tilahun − *Department of Applied Chemistry, School of Applied Natural Science, Adama Science and Technology University, 1888 Adama, Ethiopia;* ◉ orcid.org/0000-0003-1308-0292

Lemma Teshome Tufa − *Department of Applied Chemistry, School of Applied Natural Science, Adama Science and Technology University, 1888 Adama, Ethiopia;* ◉ orcid.org/0000-0001-6929-8464

Bedasa Abdisa Gonfa − *Department of Applied Chemistry, School of Applied Natural Science, Adama Science and Technology University, 1888 Adama, Ethiopia*

Taymour A. Hamdalla − *Physics Department, Faculty of Science, University of Tabuk, Tabuk 47512, KSA*

C.R. Ravikumar − *Research Centre, Department of Science, East-West Institute of Technology, Bangalore 560091, India;* ◉ orcid.org/0000-0002-4692-444X

H C Ananda Murthy − *School of Applied Sciences, Papua New Guinea University of Technology, Lae, Morobe Province 411, Papua New Guinea; Department of Prosthodontics, Saveetha Dental College & Hospital, Saveetha Institute of Medical and Technical Science (SIMATS), Saveetha University, Chennai 600077 Tamil Nadu, India;* ◉ orcid.org/0000-0002-2361-086X

Complete contact information is available at:
https://pubs.acs.org/10.1021/acsomega.4c03123

Notes

The authors declare no competing financial interest.

■ REFERENCES

(1) Kim, B. K.; Sy, S.; Yu, A.; Zhang, J.Electrochemical Supercapacitors for Energy Storage and Conversion. In *Handbook Clean Energy System*; Wiley, 2015; pp 1−25.

(2) Winter, M.; Brodd, R. J. What Are Batteries, Fuel Cells, and Supercapacitors? *Chem. Rev.* **2004**, *104* (10), 4245−4269.

(3) Hwang, J.-Y.; Myung, S.-T.; Sun, Y.-K. Sodium-Ion Batteries: Present and Future. *Chem. Soc. Rev.* **2017**, *46* (12), 3529−3614.

(4) Salinas-Torres, D.; Ruiz-Rosas, R.; Morallón, E.; Cazorla-Amorós, D. Strategies to Enhance the Performance of Electrochemical

Capacitors Based on Carbon Materials. *Front. Mater.* **2019**, *6*, No. 115, DOI: 10.3389/fmats.2019.00115.

(5) Guo, N.; Zhang, S.; Wang, L.; Jia, D. Application of Plant-Based Porous Carbon for Supercapacitors. *Acta Phys.-Chim. Sin.* **2020**, *36* (2), No. 1903055, DOI: 10.3866/PKU.WHXB201903055.

(6) Javed, M. S.; Khan, A. J.; Hanif, M.; Nazir, M. T.; Hussain, S.; Saleem, M.; Raza, R.; Yun, S.; Liu, Z. Engineering the Performance of Negative Electrode for Supercapacitor by Polyaniline Coated Fe3O4 Nanoparticles Enables High Stability up to 25,000 Cycles. *Int. J. Hydrogen Energy* **2021**, *46* (15), 9976−9987.

(7) Parida, S.; Dutta, D. P. Nanostructured Materials from Biobased Precursors for Renewable Energy Storage Applications. In *Biorenewable Nanocomposite Materials, Vol. 1: Electrocatalysts and Energy Storage*; Pathania, D.; Singh, L., Eds.; ACS Symposium Series; American Chemical Society: Washington, DC, 2022; Vol. *1410*, pp 307−366.

(8) Wang, L.; Sun, F.; Hao, F.; Qu, Z.; Gao, J.; Liu, M.; Wang, K.; Zhao, G.; Qin, Y. A Green Trace K2CO3 Induced Catalytic Activation Strategy for Developing Coal-Converted Activated Carbon as Advanced Candidate for CO2 Adsorption and Supercapacitors. *Chem. Eng. J.* **2020**, *383* (5), No. 123205.

(9) Abbas, Y.; Yun, S.; Javed, M. S.; Chen, J.; Tahir, M. F.; Wang, Z.; Yang, C.; Arshad, A.; Hussain, S. Anchoring 2D NiMoO4 Nano-Plates on Flexible Carbon Cloth as a Binder-Free Electrode for Efficient Energy Storage Devices. *Ceram. Int.* **2020**, *46* (4), 4470−4476.

(10) Wang, A.; Zheng, Z.; Li, R.; Hu, D.; Lu, Y.; Luo, H.; Yan, K. Biomass-Derived Porous Carbon Highly Efficient for Removal of Pb(II) and Cd(II). *Green Energy Environ.* **2019**, *4* (4), 414−423.

(11) Song, C.; Zhang, B.; Hao, L.; Min, J.; Liu, N.; Niu, R.; Gong, J.; Tang, T. Converting Poly(Ethylene Terephthalate) Waste into N-Doped Porous Carbon as CO2 Adsorbent and Solar Steam Generator. *Green Energy Environ.* **2022**, *7* (3), 411−422.

(12) Gong, J.; Liu, J.; Chen, X.; Jiang, Z.; Wen, X.; Mijowska, E.; Tang, T. Converting Real-World Mixed Waste Plastics into Porous Carbon Nanosheets with Excellent Performance in the Adsorption of an Organic Dye from Wastewater. *J. Mater. Chem. A* **2015**, *3* (1), 341−351.

(13) Yuan, X.; Cho, M. K.; Lee, J. G.; Choi, S. W.; Lee, K. B. Upcycling of Waste Polyethylene Terephthalate Plastic Bottles into Porous Carbon for CF4 Adsorption. *Environ. Pollut.* **2020**, *265*, No. 114868.

(14) Ma, J.; Liu, J.; Song, J.; Tang, T. Pressurized Carbonization of Mixed Plastics into Porous Carbon Sheets on Magnesium Oxide. *RSC Adv.* **2018**, *8* (5), 2469−2476.

(15) Cheng, Y.; Wu, L.; Fang, C.; Li, T.; Chen, J.; Yang, M.; Zhang, Q. Synthesis of Porous Carbon Materials Derived from Laminaria Japonica via Simple Carbonization and Activation for Supercapacitors. *J. Mater. Res. Technol.* **2020**, *9* (3), 3261−3271.

(16) Yan, K.; Li, R.; Yang, Z.; Li, X.; Wang, Y.; Wu, G. Biomass Waste-Derived Porous Carbon Efficient for Simultaneous Removal of Chlortetracycline and Hexavalent Chromium. *iScience* **2021**, *24* (5), No. 102421.

(17) González-García, P.; Gamboa-González, S.; Andrade Martínez, I.; Hernández-Quiroz, T. Preparation of Activated Carbon from Water Hyacinth Stems by Chemical Activation with K 2 CO 3 and Its Performance as Adsorbent of Sodium Naproxen. *Environ. Prog. Sustainable Energy* **2020**, *39* (3), No. e13366, DOI: 10.1002/ep.13366.

(18) Sivachidambaram, M.; Vijaya, J. J.; Kennedy, L. J.; Jothiramalingam, R.; Al-Lohedan, H. A.; Munusamy, M. A.; Elanthamilan, E.; Merlin, J. P. Preparation and Characterization of Activated Carbon Derived from the: Borassus Flabellifer Flower as an Electrode Material for Supercapacitor Applications. *New J. Chem.* **2017**, *41* (10), 3939−3949.

(19) Hou, J.; Liu, Y.; Wen, S.; Li, W.; Liao, R.; Wang, L. Sorghum-Waste-Derived High-Surface Area KOH-Activated Porous Carbon for Highly Efficient Methylene Blue and Pb(II) Removal. *ACS Omega* **2020**, *5* (23), 13548−13556, DOI: 10.1021/acsomega.9b04452.

(20) Kurniawan, F.; Wongso, M.; Ayucitra, A.; Soetaredjo, F. E.; Angkawijaya, A. E.; Ju, Y.-H.; Ismadji, S. Carbon Microsphere from Water Hyacinth for Supercapacitor Electrode. *J. Taiwan Inst. Chem. Eng.* **2015**, *47* (5), 197−201.

(21) Saning, A.; Herou, S.; Dechtrirat, D.; Ieosakulrat, C.; Pakawatpanurut, P.; Kaowphong, S.; Thanachayanont, C.; Titirici, M.-M.; Chuenchom, L. Green and Sustainable Zero-Waste Conversion of Water Hyacinth (*Eichhornia Crassipes*) into Superior Magnetic Carbon Composite Adsorbents and Supercapacitor Electrodes. *RSC Adv.* **2019**, *9* (42), 24248−24258.

(22) Sánchez-Monreal, J.; Vera, M.; García-Salaberri, P. A. Fundamentals of Electrochemistry with Application to Direct Alcohol Fuel Cell Modeling. In *Proton Exchange Membrane Fuel Cell*; IntechOpen, 2018; Vol. *13*, p 729.

(23) Román, S.; Ledesma, B.; Álvarez, A.; Coronella, C.; Qaramaleki, S. V. Suitability of Hydrothermal Carbonization to Convert Water Hyacinth to Added-Value Products. *Renewable Energy* **2020**, *146* (6), 1649−1658.

(24) Ananpreechakorn, W.; Seetawan, T. Synthesis and Characterization of Activated Carbon from Water Hyacinth. *J. Phys.: Conf. Ser.* **2021**, *2013* (1), No. 012025.

(25) González-García, P.; Gamboa-González, S.; Andrade Martínez, I.; Hernández-Quiroz, T. Preparation of Activated Carbon from Water Hyacinth Stems by Chemical Activation with K 2 CO 3 and Its Performance as Adsorbent of Sodium Naproxen. *Environ. Prog. Sustainable Energy* **2020**, *39* (3), No. e13366, DOI: 10.1002/ep.13366.

(26) Boonprachai, R.; Autthawong, T.; Namsar, O.; Yodbunork, C.; Yodying, W.; Sarakonsri, T. Natural Porous Carbon Derived from Popped Rice as Anode Materials for Lithium-Ion Batteries. *Crystals* **2022**, *12* (2), No. 223, DOI: 10.3390/cryst12020223.

(27) Hernández-Rentero, C.; Marangon, V.; Olivares-Marín, M.; Gómez-Serrano, V.; Caballero, Á.; Morales, J.; Hassoun, J. Alternative Lithium-Ion Battery Using Biomass-Derived Carbons as Environmentally Sustainable Anode. *J. Colloid Interface Sci.* **2020**, *573*, 396−408.

(28) Kouahou, G. N.; Fotsop, C. G.; Amola, L. A.; Atemkeng, C. D.; Tamo, A. K.; Kenda, G. T.; Tagne, R. F. T.; Kamgaing, T. Optimized Preparation of Activated Carbon with High Porosities Based on Puck Shells (Afrostyrax Lepidophyllus) by Response Surface Methodology and Physico-Chemical Characterization. *R. Soc. Open Sci.* **2023**, *10* (12), 682−687, DOI: 10.1098/rsos.230911.

(29) Morales S, L.; Baas-López, J. M.; Barbosa, R.; Pacheco, D.; Escobar, B. Activated Carbon from Water Hyacinth as Electrocatalyst for Oxygen Reduction Reaction in an Alkaline Fuel Cell. *Int. J. Hydrogen Energy* **2021**, *46* (51), 25995−26004.

(30) Fregue, T. T. R.; Ionel, I.; Gabche, A. S.; Mihaiuti, A.-C. Optimization of the Activated Carbon Preparation from Avocado Seeds, Using the Response Surface Methodology. *Rev. Chim.* **2019**, *70* (2), 410−416.

(31) Abou- Elyazed, A. S.; Hassan, S.; Ashry, A. G.; Hegazy, M. Facile, Efficient, and Cheap Electrode Based on SnO 2 /Activated Carbon Waste for Supercapacitor and Capacitive Deionization Applications. *ACS Omega* **2022**, *7* (23), 19714−19720.

(32) Zhao, T.; Yao, Y.; Yuan, Y.; Wang, M.; Wu, F.; Amine, K.; Lu, J. A Universal Method to Fabricating Porous Carbon for Li-O2 Battery. *Nano Energy* **2021**, *82* (7), No. 105782.

(33) Gao, Z.; Yun, S.; Yang, C.; Zhang, Y.; Dang, J.; Yang, G.; Yang, T.; Qiao, D.; Wang, K. Niobium- and Cobalt-Modified Dual-Source-Derived Porous Carbon with a Honeycomb-like Stable Structure for Supercapacitor and Hydrogen Evolution Reaction. *J. Colloid Interface Sci.* **2023**, *639* (1), 33−48.

(34) Fite, M. C.; Wang, P.-J.; Imae, T. Symmetric and Asymmetric Supercapacitors of ITO Glass and Film Electrodes Consisting of Carbon Dot and Magnetite. *Batteries* **2023**, *9* (3), No. 162, DOI: 10.3390/batteries9030162.

(35) Ban, S.; Zhang, J.; Zhang, L.; Tsay, K.; Song, D.; Zou, X. Charging and Discharging Electrochemical Supercapacitors in the

Presence of Both Parallel Leakage Process and Electrochemical Decomposition of Solvent. *Electrochim. Acta* **2013**, *90*, 542−549.

(36) de Oliveira Cremonezzi, J. M.; Tiba, D. Y.; Domingues, S. H. Fast Synthesis of δ-MnO2 for a High-Performance Supercapacitor Electrode. *SN Appl. Sci.* **2020**, *2* (10), No. 1689, DOI: 10.1007/s42452-020-03488-2.

(37) Januszewicz, K.; Cymann-Sachajdak, A.; Kazimierski, P.; Klein, M.; Łuczak, J.; Wilamowska-Zawłocka, M. Chestnut-Derived Activated Carbon as a Prospective Material for Energy Storage. *Materials* **2020**, *13* (20), No. 4658, DOI: 10.3390/ma13204658.

(38) Huarote-Garcia, E.; Cardenas-Riojas, A. A.; Monje, I. E.; López, E. O.; Arias-Pinedo, O. M.; Planes, G. A.; Baena-Moncada, A. M. Activated Carbon Electrodes for Supercapacitors from Purple Corncob (*Zea Mays* L.). *ACS Environ. Au* **2024**, *4* (2), 80−88.

(39) Reddygunta, K. K. R.; Beresford, R.; Šiller, L.; Berlouis, L.; Ivaturi, A. Activated Carbon Utilization from Corn Derivatives for High-Energy-Density Flexible Supercapacitors. *Energy Fuels* **2023**, *37* (23), 19248−19265.

(40) Zhang, F.; Xiao, X.; Gandla, D.; Liu, Z.; Tan, D. Q.; Ein-Eli, Y. Bio-Derived Carbon with Tailored Hierarchical Pore Structures and Ultra-High Specific Surface Area for Superior and Advanced Supercapacitors. *Nanomaterials* **2022**, *12* (1), No. 27, DOI: 10.3390/nano12010027.

(41) Deckenbach, D.; Schneider, J. J. A Long-Overlooked Pitfall in Rechargeable Zinc−Air Batteries: Proper Electrode Balancing. *Adv. Mater. Interfaces* **2023**, *10* (15), 1765−1780.

(42) Alves, A. C. F.; Antero, R. V. P.; de Oliveira, S. B.; Ojala, S. A.; Scalize, P. S. Activated Carbon Produced from Waste Coffee Grounds for an Effective Removal of Bisphenol-A in Aqueous Medium. *Environ. Sci. Pollut. Res.* **2019**, *26* (24), 24850−24862.

(43) Emamy, F. H.; Bumajdad, A.; Lukaszewicz, J. P. Adsorption of Hexavalent Chromium and Divalent Lead Ions on the Nitrogen-Enriched Chitosan-Based Activated Carbon. *Nanomaterials* **2021**, *11* (8), No. 1907, DOI: 10.3390/nano11081907.

(44) Lawtae, P.; Tangsathitkulchai, C. A New Approach for Controlling Mesoporosity in Activated Carbon by the Consecutive Process of Air Oxidation, Thermal Destruction of Surface Functional Groups, and Carbon Activation (the OTA Method). *Molecules* **2021**, *26* (9), No. 2758, DOI: 10.3390/molecules26092758.

(45) Rahma, N. A.; Kurniasari, A.; Pambudi, Y. D. S.; Bintang, H. M.; Zulfia, A.; Hudaya, C. Characteristics of Corncob-Originated Activated Carbon Using Two Different Chemical Agent. *IOP Conf. Ser.: Mater. Sci. Eng.* **2019**, *622* (1), No. 012030, DOI: 10.1088/1757-899X/622/1/012030.

(46) Feng, P.; Li, J.; Wang, H.; Xu, Z. Biomass-Based Activated Carbon and Activators: Preparation of Activated Carbon from Corncob by Chemical Activation with Biomass Pyrolysis Liquids. *ACS Omega* **2020**, *5* (37), 24064−24072.

(47) Mojoudi, N.; Mirghaffari, N.; Soleimani, M.; Shariatmadari, H.; Belver, C.; Bedia, J. Phenol Adsorption on High Microporous Activated Carbons Prepared from Oily Sludge: Equilibrium, Kinetic and Thermodynamic Studies. *Sci. Rep.* **2019**, *9* (1), No. 19352.

(48) Mirabelle, A.; Ngueabouo, S.; Tiegam, F. Provide Better Carbon Properties with Large Specific Surface Areas. *Mater. Adv.* **2022**, *3*, 8361−8374, DOI: 10.1039/d2ma00591c.

(49) Wang, X.; Yun, S.; Fang, W.; Zhang, C.; Liang, X.; Lei, Z.; Liu, Z. Layer-Stacking Activated Carbon Derived from Sunflower Stalk as Electrode Materials for High-Performance Supercapacitors. *ACS Sustainable Chem. Eng.* **2018**, *6* (9), 11397−11407.

(50) Diantoro, M.; Istiqomah, I.; Fath, Y. Al.; Mufti, N.; Nasikhudin, N.; Meevasana, W.; Alias, Y. B. Hierarchical Activated Carbon−MnO2 Composite for Wide Potential Window Asymmetric Supercapacitor Devices in Organic Electrolyte. *Micromachines* **2022**, *13* (11), No. 1989, DOI: 10.3390/mi13111989.

(51) Dos Reis, G. S.; Larsson, S. H.; de Oliveira, H. P.; Thyrel, M.; Lima, E. C. Sustainable Biomass Activated Carbons as Electrodes for Battery and Supercapacitors−a Mini-Review. *Nanomaterials* **2020**, *10* (7), No. 1398, DOI: 10.3390/nano10071398.

(52) Zhang, H.; Cao, G.; Yang, Y.; Gu, Z. Capacitive Performance of an Ultralong Aligned Carbon Nanotube Electrode in an Ionic Liquid at 60°C. *Carbon* **2008**, *46* (1), 30−34.

(53) Chun, S.-E.; Whitacre, J. F. Formation of Micro/Mesopores during Chemical Activation in Tailor-Made Nongraphitic Carbons. *Microporous Mesoporous Mater.* **2017**, *251* (24), 34−41.

(54) Balasubramanian, M. M.; Subramani, M.; Murugan, D.; Ponnusamy, S. Groundnut Shell−Derived Porous Carbon-Based Supercapacitor with High Areal Mass Loading Using Carbon Cloth as Current Collector. *Ionics* **2020**, *26* (12), 6297−6308, DOI: 10.1007/s11581-020-03754-8.

(55) Barakat, N. A. M.; Mahmoud, M. S.; Moustafa, H. M. Comparing Specific Capacitance in Rice Husk-Derived Activated Carbon through Phosphoric Acid and Potassium Hydroxide Activation Order Variations. *Sci. Rep.* **2024**, *14* (1), No. 1460.

(56) Yang, C.; Yun, S.; Shi, J.; Sun, M.; Zafar, N.; Arshad, A.; Zhang, Y.; Zhang, L. Tailoring the Supercapacitive Behaviors of Co/Zn-ZIF Derived Nanoporous Carbon via Incorporating Transition Metal Species: A Hybrid Experimental-Computational Exploration. *Chem. Eng. J.* **2021**, *419*, No. 129636.

(57) Vu, D.-L.; Seo, J.-S.; Lee, H.-Y.; Lee, J.-W. Activated Carbon with Hierarchical Micro−Mesoporous Structure Obtained from Rice Husk and Its Application for Lithium−Sulfur Batteries. *RSC Adv.* **2017**, *7* (7), 4144−4151.

(58) Salleh, N. A.; Kheawhom, S.; Mohamad, A. A. Character-izations of Nickel Mesh and Nickel Foam Current Collectors for Supercapacitor Application. *Arab. J. Chem.* **2020**, *13* (8), 6838−6846.

(59) Tong, Y.; Yang, J.; Li, J.; Cong, Z.; Wei, L.; Liu, M.; Zhai, S.; Wang, K.; An, Q. Lignin-Derived Electrode Materials for Super-capacitor Applications: Progress and Perspectives. *J. Mater. Chem. A* **2023**, *11* (3), 1061−1082.

(60) Shrestha, D.; Rajbhandari, A. The Effects of Different Activating Agents on the Physical and Electrochemical Properties of Activated Carbon Electrodes Fabricated from Wood-Dust of Shorea Robusta. *Heliyon* **2021**, *7* (9), No. e07917.